ISSN 1392–1207. MECHANIKA. 2020 Volume 26(3): 183–190

Uniaxial Tensile Behaviour of 75 µm Thick Stainless-Steel Foils

Lin WANG
Hefei University, Hefei, 230061, China, E-mail: linw@mail.smu.edu

crossref http://dx.doi.org/10.5755/j01.mech.26.3.23417

1. Introduction

75 µm thick stainless-steel foils AISI 304L and 439 are under consideration for potential bipolar plates in automotive fuel-cell assembly. Precise knowledges of their mechanical properties are essentially important for design, fabrication and reliability prediction of such product. As foil thickness becomes comparable with its grain size, the deformation behaviour and ductile fracture of metal foils could accordingly change [1-13]. The size effects of material properties are found closely related to specimen size, geometry [1-6, 11-13] and material microstructures [2-4, 7, 13].

Uniaxial tension test, for instance, is intensively applied to reveal the mechanical properties of foil material in micro/meso scale [1-13]. The derived stress-strain relations from such test are useful for mechanical properties identification. Challenge in such test is to precisely measure the axial strain of foil specimen at micro/meso scale [5, 6]. Two approaches are commonly found for axial strain measurement of foil materials. In the first approach, mechanical extensometer was used to obtain the axial elongation of the testing specimen [2, 4, 7, 13]. However, fatal damage could be introduced by the mechanical mounting of extensometer due to specimen fragility. Alternatively, researchers usually directly treat the displacement of loading crosshead equal as the axial elongation of foil specimen over its entire gage section [1, 3, 5, 6, 8-12]. Although much simpler, serious measurement errors were introduced into specimen elongation due to system compliance and specimen deformation outside its gage section [5, 6]. Furthermore, the post-necking stress-strain curve of foil specimen should be carefully calibrated as the stress state within the growing neck deviates from the uniform uniaxial tension [14, 15]. An accurate and relatively simple strain measurement technique, such as digital image correlation (DIC) method, is therefore recommended to obtain more convinced mechanical properties of foil specimens [6]. The DIC-based technique is widely used to characterize material behavior [14-18], but is seldomly applied for foil materials in small size scale [4, 11].

In this presented work, the mechanical behaviors of 75 µm thick stainless-steel foils AISI 304L and 439 under uniaxial tension were studied using DIC-based full-field deformation measurement technique. The true stress-strain curves of foil materials till fracture derived from different measurement methods were critically compared. The influences of material microstructure on the mechanical properties of foil materials were accessed. The overall objective of this work is to achieve a better mechanical characterization of foil materials in small size scale by using a technically simple and robust strain measurement method.

2. Experiment

The 75 µm thick cold-rolled stainless-steel foils FCC AISI304L and BCC AISI439 were supplied from General Motors R&D Center. The nominal chemical compositions are listed in Table 1. Detailed microstructures and textures of foils were characterized by SEM. Dog-bone tensile test specimens (Fig. 1) were prepared by photochemical etching technique (dimension tolerance ±0.025 mm). The axial direction of specimens was aligned to rolling (RD) or transverse directions (TD) of foil to investigate its anisotropy. Some specimens were annealed in a vacuum environment at 1050°C for 15 minutes to identify the effect of heat treatment on the microstructural and mechanical behaviors of foil materials.

Table 1

Chemical compositions of 75µm thick stainless-steel foils

	Cr	Ti	Mn	Si	Ni	Al	P	C	S	N	Fe
AISI 304L	18		≤2	≤0.75	8.9		≤0.04	≤0.03	≤0.015		balanced
AISI 439	17.9	0.7	≤1	≤1	≤0.5	≤0.15	≤0.04	≤0.03	≤0.03	≤0.03	balanced

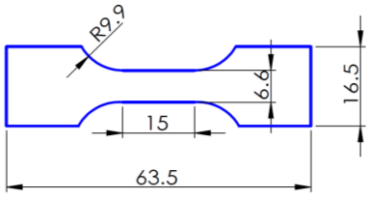

Fig. 1 Schematic of the tensile test specimen

Uniaxial tensile tests of 75 µm thick foil specimens were performed on Instron E1000 testing machine (±1000 N load capacity, ±0.1 N accuracy) at room temperature. The tensile loading was controlled by constant crosshead speed, corresponding to a nominal strain rate around 1×10^{-3}/s. A small preload resulting in about 30 MPa axial engineering stress was imposed on the specimen to guarantee a flat specimen surface for image acquisition. At least 3 specimens were tested for each orientation, heat treatment and material. To facilitate DIC-based deformation measurement, one surface of the tensile specimen was decorated with fine black-to-white speckles by spraying thin but uniform paint droplets with spatial resolution of digital images as ~0.034 mm per pixel. High-quality contrast pattern on specimen surface

was digitally imaged continuously by a CCD camera (acquisition rate 3fps) during the tensile testing. The captured digital images (1280×960 pixels, 8 bit) were then processed for specimen deformation measurement by the non-contact DIC algorithm Ncorr [19]. Subset radius for DIC processing was set as 20 pixels with a grid spacing of 2 pixels. Based on the acquired digital images before the start of the tensile test, error in the local strain measurement is estimated to be about 0.03 %-0.05 % at most [20].

The axial engineering and true strain based on crosshead displacement D over the initial gage length L_0 [1, 3, 5, 6, 8, 12] was calculated as:

$$e = D / L_0, \varepsilon = ln(1+e). \tag{1}$$

The axial true strain of foil specimen was also measured using two definitions based on DIC strain data [21-23]. Following the tensile test methodology, the first definition was averaging the axial true strain $\varepsilon(i, j)$ at each grid point (i, j) obtained via DIC over the entire gage section:

$$\varepsilon^1 = \frac{1}{MN}\sum_{j=1}^{N}\sum_{i=1}^{M}\varepsilon(i, j), \tag{2}$$

where: M and N are the total numbers of grid points along the selected gage length and width directions. In the second definition, the axial strain was defined by:

$$\varepsilon^3 = \frac{1}{N}\sum_{j=1}^{N}\varepsilon(M_0, j), \tag{3}$$

where: ε^3 is the axial local strain averaged along the cross-section with the smallest width (i.e., the neck centerline at $I=M_0$), but not necessarily perfectly normal to the loading direction. This definition has been proven effectively characterize the local stress-strain relation, especially at large strain level [21-23]. The true uniaxial stress was computed from:

$$\sigma = \frac{Fe^{\varepsilon}}{A_0}, \tag{4}$$

where: ε is the true strain measured from Eqs. (1), (2) or (3), and A_0 is the original cross-section area of tensile specimen.

3. Results

3.1. Microstructural characterization

The microstructure of the as-received stainless-steel foils in the surface plane (RD×TD) by electron backscatter diffraction (EBSD) is shown in Fig. 2. As shown in Fig. 2, a, twins appear intensively within grains for the FCC AISI 304L foil so the average grain size is 3.76 μm considering twins or 7.13 μm if disregarding twins. Twins are hardly observed in the as-received BCC AISI 439 foil (Fig. 2, b) with average grain size of 19.23 μm. The annealed AISI 304L foil was found dramatically coarse-grained. The average grain size of AISI 304L foils after annealing is 16.8 μm including twins or 36.8 μm excluding twins based on EBSD data analysis (Fig. 2, c). On the other hand, the AISI 439 foil after annealing has an average grain size about 21.5 μm (Fig. 2, d), closing to the grain size of as-received foil. The textures of as-received foils are shown in Fig. 3 by inverse pole figures (IPF). The IPF map indicates an almost random texture for AISI 304L foil, while the AISI 439 foils show a strong {111} texture. Limited change in textures is found for both foil materials after heat treatment.

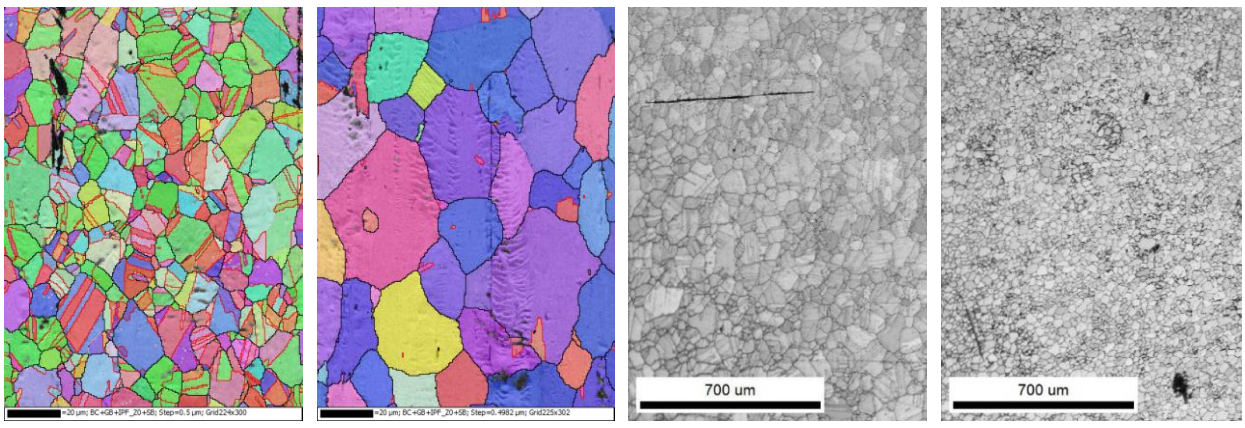

a b c d

Fig. 2 EBSD measured microstructure of the as-received stainless-steel foils: a) AISI 304L; b) AISI 439; c) annealed AISI 304L; d) annealed AISI 439

3.2. Plastic deformation

The plastic deformation of foil specimens during the tensile test was quantified using DIC-based algorithm Ncorr [32]. The axial true plastic strain contours ε_x measured by DIC method of one AISI 439 foil specimen over its entire gage section in deformed configuration are shown in Fig. 4, comparing between images captured at t = 312.9 s (peak load), 391.6 s, 426.3 s, 434 s (the last image just prior ductile fracture) and the reference image captured at 46.1 s (around material proportional limit) (Fig. 4, a). Based on the strain measurement data, the axial plastic strain maps over the centered gage section are relatively uniform at peak load point (Fig. 4, b). Beyond that point, a diffuse neck is gradually formed in the center portion of the specimen. The cumulative strain contour of the image just prior to the ductile

rupture (Fig. 4, e) shows an inclined narrow deformation band (dashed line) with an angle of 54.1° respect to the loading direction. The maximum axial true plastic strain ε_x^{max} at this load step is at least 0.570, much higher than the average value of 0.372 within the centered 60% gage section at the same load step. The incremental axial true plastic strain map compared between the images captured at t = 426.3 s and 434 s is shown in Fig. 4, f. The incremental axial true plastic strain map compared between the images captured at t = 426.3 s and 434 s is shown in Fig. 4, f. The inclined narrow deformation band indicates the localized necking, which is coincident to the final fracture surfaces.

Similarly, the axial true plastic strain ε_x of one specimen of AISI 304L foil material over its entire gage section was also analyzed by DIC technique. The cumulative true plastic strain maps between images captured at t =503.4 s (peak load), 513.3 , 519.8 , 521.6 s (the last image just prior ductile fracture) and the reference image at 35 s (around proportional limit) are shown in Fig. 5. Different from AISI 439 foils, the AISI 304L foil specimen experienced a rather shorter loading stage from peak load point to the final ductile fracture (Fig. 5, a). Based on DIC measurement, the axial deformation of AISI 304L specimen at the peak load point cannot be statistically treated as homogenous. The average value of plastic strain ε_x^{ave} over the region of interest at t=521.6 s is 0.659, while the maximum plastic strain ε_x^{max} is 0.833 (Fig. 5, e). The incremental strain map between the last two images shows an inclined narrow deformation band (Fig. 5, f) with an angle of 56.2° respect to the loading direction. Although an inclined narrow deformation band was formed within gage section, the final fracture surfaces of AISI 304L foil specimens are almost normal to the tensile direction (Fig. 5, f).

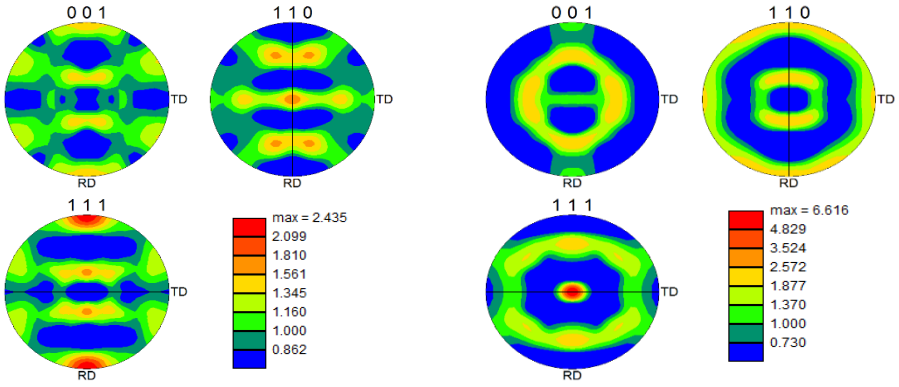

a b

Fig. 3 Inverse pole figure maps of stainless-steel foils: a) AISI 304L and b) AISI 439

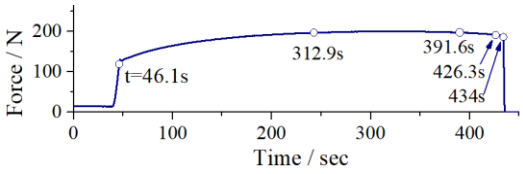

a

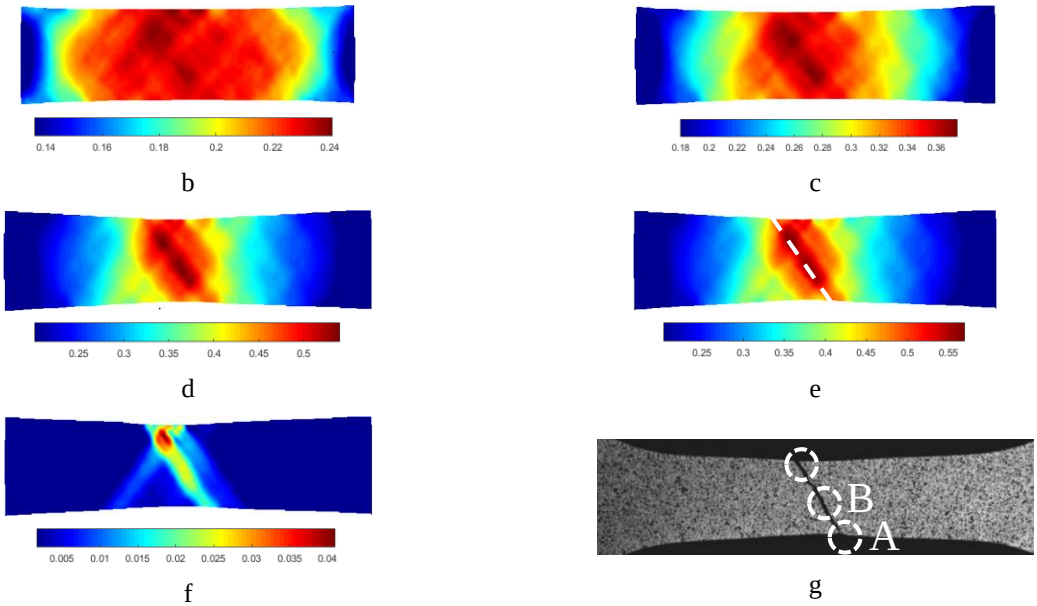

b c d e f g

Fig. 4 a) Force history curve of an as-received AISI439 foil specimen, where the circles indicate the acquisition time of selected images for DIC deformation measurement. The cumulative plastic true strain distributions at increasing time are shown in b), c), d), and e); f) the incremental plastic true strain between d) and e); g) fractured specimen

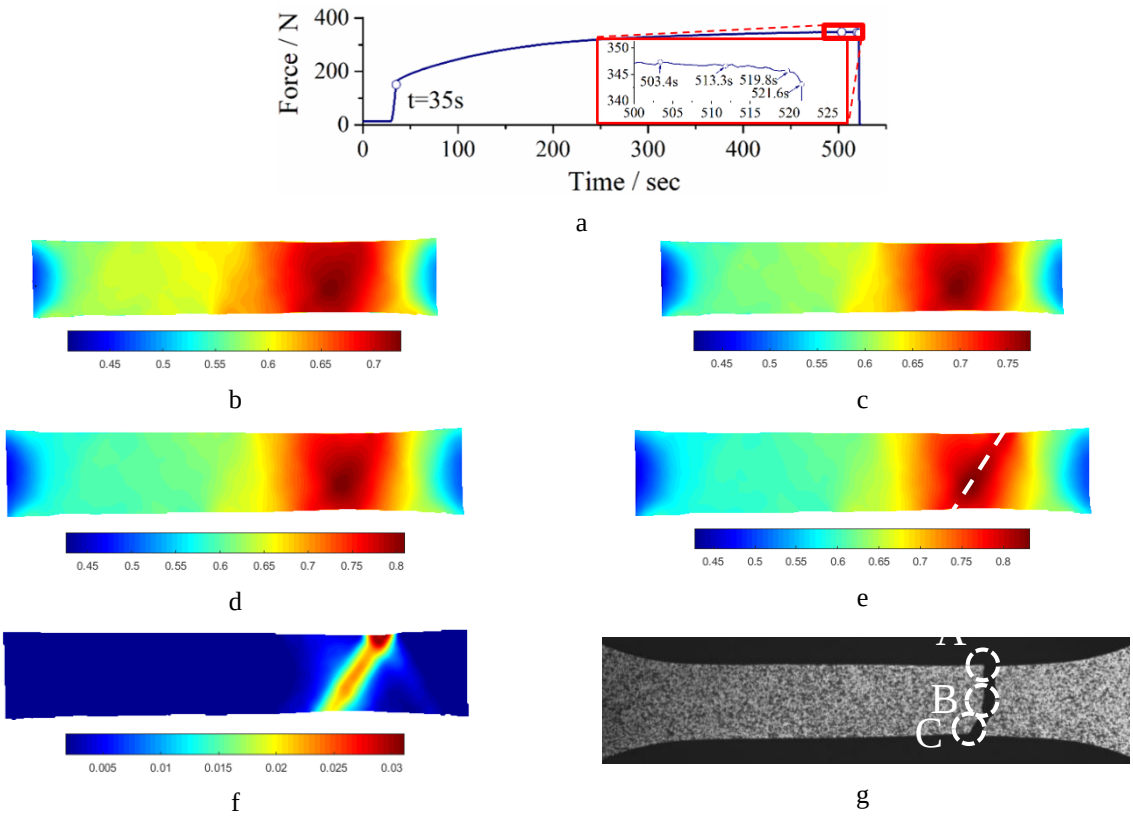

Fig. 5 a) Force history curve of an as-received AISI304L foil specimen with circles indicating the acquisition time of selected images for DIC deformation measurement. The cumulative plastic true strain distributions at increasing time shown in in b), c), d) and e); f) the incremental plastic true strain between d) and e); g) fractured specimen

3.3. Fracture morphology

Ductile metal material usually fails in a consequence of uniform deformation, diffuse necking, crack development from specimen inside, shear formation and final separation of material. Detailed morphologies of fracture surfaces were captured by SEM and shown in Fig. 6. The tensile failure mode is found predominant for AISI 304L foil specimen in either rolling or transverse direction. Rough and

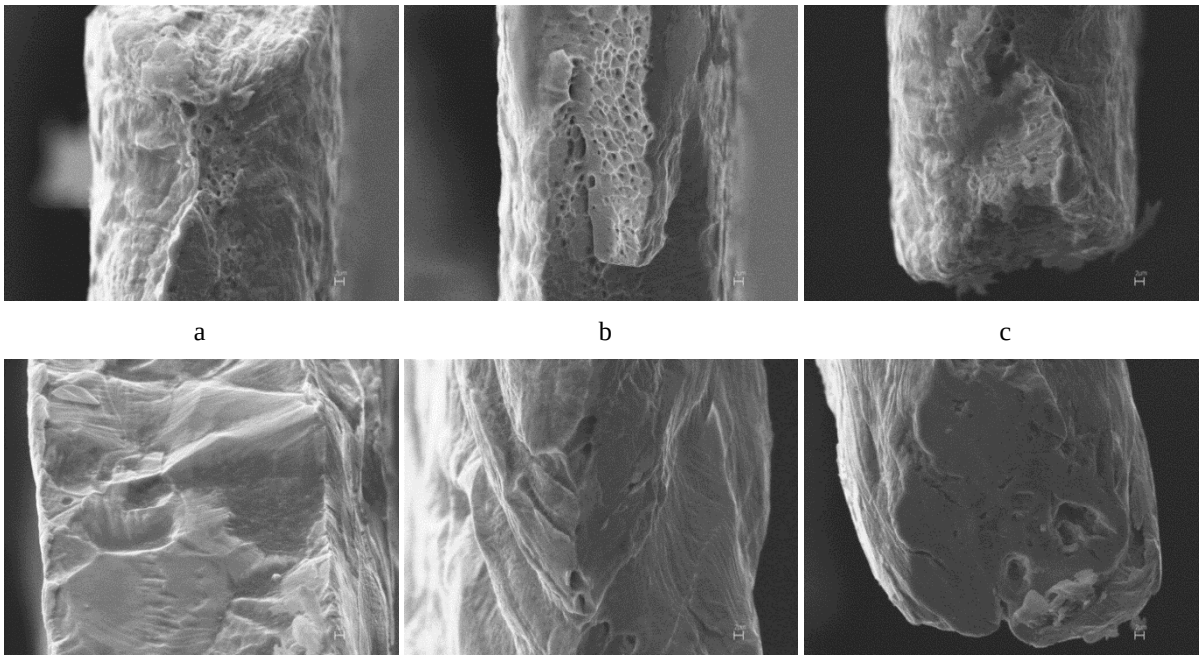

Fig. 6 SEM fracture morphologies (3000×) of as-received AISI304L foil in (a) the initiation, (b) middle and (c) end of the fracture surface. Fracture morphologies (3000×) of as-received AISI439 foil in the initiation, middle and end of the fracture surface are shown in d), e) and f). The corresponding positions are shown in Fig. 4, g and Fig. 5, g as A, B, and C

dimpled fracture surfaces with many fine voids are typically observed for the as-received AISI304L specimen. Though just a short deformation stage experienced between the peak load and the failure points, void nucleation and growth developed well due to high-level tensile stress which dominating the ductile fracture of AISI304L foil. Comparing to the other two locations, the fracture surface around the failure initiation site is much narrow and irregular (Fig. 6, a).

Shear failure mode dominants for AISI 439 foil material. The shear fracture surfaces usually incline at an angle of 43°-62° with respect to the tensile loading direction. The fracture surfaces of as-received SS439 are typically rough with many small ridges. Only a few relatively large voids if any are observed on the fracture surface at some locations (Fig. 6, e and f). Since as-received SS439 foils are coarse-grained already so these flat fracture surfaces may also be the grain boundaries or facets of grains. There was typically a rather extensive diffuse necking deformation stage between the peak load and the ductile failure in as-received SS439 specimen, with a single narrow deformation (Fig. 4, e). The sever shearing in such a very narrow band dominated the ductile fracture process without significant tension-induced void nucleation and growth in as-received SS439 foils. Specimen orientations and heat treatment show no obvious influence on the failure mode of both foil materials.

4. Discussion

4.1. Effect of strain measurement methods

The axial strain of foil specimen ε_x if deriving from crosshead displacement consists of axial strain components within and outside specimen gage section ε_{x1} and ε_{x2}, and namely, contribution from system compliance ε_{x3} [5, 6] or:

$$\varepsilon_x = \varepsilon_{x1} + \varepsilon_{x2} + \varepsilon_{x3}. \quad (5)$$

The axial strain ε_{x1} derived from axial elongation within specimen gage section is a sum of three components:

$$\varepsilon_{x1} = \varepsilon_{x1e} + \varepsilon_{x1u} + \varepsilon_{x1n}, \quad (6)$$

where: ε_{x1e} is the elastic strain, ε_{x1u} the uniform plastic strain and ε_{x1n} the post-necking plastic strain. For ductile foil materials, the elastic strain ε_{x1e} is usually negligible. The uniform plastic strain ε_{x1u} or the onset of the diffuse neck is determined by Considère criterion.

Fig. 7 compares the true stress-strain curves of foil materials following the DIC-based strain measurement methods as Eqs.(1) to (3). The flow stress of AISI 304L specimen obtained from crosshead displacement (solid navy curve in Fig.7, a) is up to 9% lower than the results from DIC data when the true strain smaller than 0.4. This is because that the stress-strain curve derived from crosshead displacement fails to exclude the components ε_{x2} and ε_{x3} caused by the specimen deformation outside gage section and respectively, the system compliance. The overestimated axial strain will in turn shift the resulted stress-strain curve relatively lower. With increasing strain, the deviation in stress-strain curves becomes smaller as ε_{x2} and ε_{x3} contribute less to the total axial strain ε_x The uniform strain ε_{x1u} of stress-strain relations based on crosshead displacement and DIC measurement averaged over entire gage length are respectively 0.612 and 0.658 (circles in Fig. 7, a). The difference in uniform strain reveals the combined contribution of ε_{x2} and ε_{x3} at this applied stress level. The two DIC-based stress-strain curves are almost overlapped till the onset strain of diffuse neck. Beyond that, the stress-strain curve based on DIC local strain Eq. (3) extends to a fracture strain 0.814 (solid red curve). The fracture strain from crosshead displacement is only 0.682 (solid navy curve), as the total nonuniform elongation of specimen and its system compliance displacement are averaged over the entire gage length.

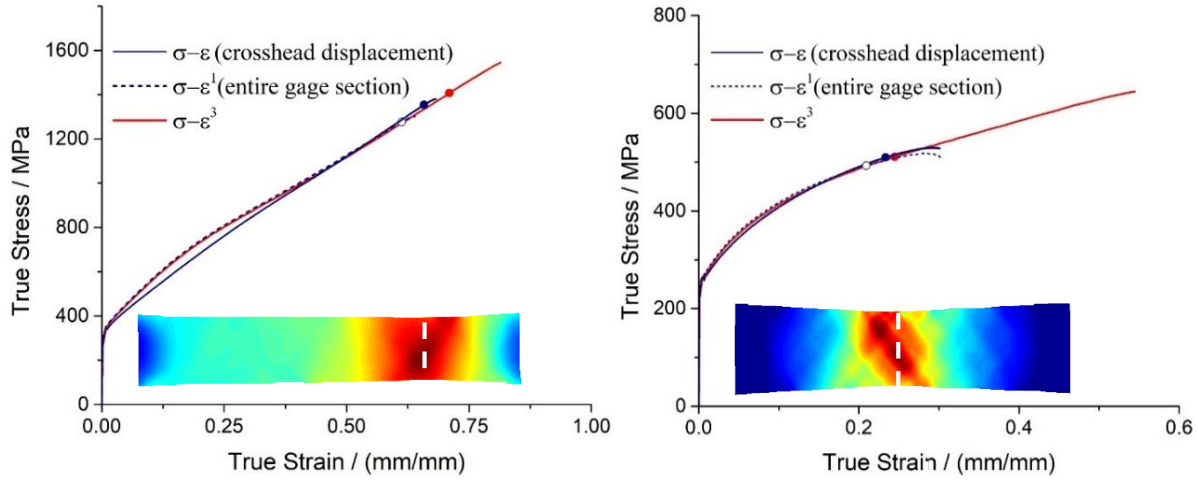

a b

Fig. 7 True stress-strain curves of foil material: a) AISI304L and b) AISI439 calculated using Eqs. (1) to (3), with circles indicating the onset of the diffuse neck. The dashed line is the smallest cross section for DIC based local strain measurement

The stress-strain curves of AISI439 foil material obtained from crosshead displacement (solid navy curve) and DIC measurements over entire gage section (dashed navy curve) diverge slightly from each other (Fig. 7, b). The

combined contribution in axial strain due to system compliance and deformation outside the gage section is relatively small when the stress applied on AISI439 specimen is much lower compared to the applied stress on AISI304L specimen. The uniform strain ε_{x1u} determined from these two curves are respectively 0.209 and 0.233. The two stress-strain curves based on DIC measurements are found almost coincident till the onset of the diffuse neck. The fracture strain is measured as 0.5446 from DIC based local stress-strain relation, 2.23 times of its uniform strain as 0.245.

With DIC technique, one can directly focus on the specimen deformation only over its gage section, the results interested. Based on the comparison of stress-strain curves, the results obtained by DIC technique can effectively eliminate the influences of system compliance and deformation undertaken outside of specimen gage section. Both factors will make the flow stress curves of foil specimen underestimated if deriving from the crosshead displacement.

As the stress state of foil specimen increasingly deviates from the uniaxial tensile condition, the stress-strain relation beyond the onset of diffuse necking becomes inaccurate. The DIC based local axial strain measurement method also extend the stress-strain curve to the maximum strain of 0.814 and 0.545 respectively for AISI 304L and AISI 439 foils, that are about 1.33 and 2.23 times of the onset of diffuse necking. This extended strain hardening behavior of foil materials at large strains is often needed in analyzing strain localization and ductile failure in the microforming process. Though some inverse correlation methods can also extract the post-necking strain hardening behavior of foil material, the applied DIC measurement method in this work is much simpler with acceptable accuracy.

4.2 Effect of microstructures

The true stress-strain curves of foil specimens with loading direction aligned to transverse direction and of the annealed specimens are shown in Fig.8. Strain data of all curves are determined using the DIC local strain measurements Eq. (3). Obtained 0.2% offset yield stress, fracture strength and strain are summarized in Table 2. Although no strong statistical basis for comparison of values associated with the specimen orientation and heat treatment, the reported data in Table 2 is believed to be representative of mechanical properties of foil materials AISI 304L and AISI 439 under quasi-static tensile at room temperature. AISI 304L foil shows no obvious anisotropic mechanical property based on the stress-strain curves (Fig. 8, a) and statistical results. After annealing, the yield and flow stress, fracture strength and strain of AISI 304L specimen are significantly reduced. This change attributes to the obvious increment in grain size after heat-treat processing. The AISI 439 foil specimen aligned to transverse direction is about 3-4% larger in yield and flow stress compared to the rolling direction (Fig. 8, b), indicating an evident anisotropy in material behaviours. The global flow stress of annealed AISI 439 foil material keeps consistent to the as-received material, but dramatic decrement of material ductility is observed in Fig. 7, b. The yield phenomenon of annealed AISI 439 foil specimen becomes more significant compared to as-received specimens, showing a change in dislocation density is introduced by heat treatment.

As observed from Fig. 8, the differences in microstructure, such as grain size and shape, texture and dislocation distributions yield obvious different mechanical behaviors for foil materials. The as-received AISI 304L foil specimens with respect to rolling and transverse directions behaved almost coincident in stress-strain relations. This is attributed to the almost random texture of foil material. The applied heat treatment at 1050°C for 15 minutes caused a recrystallization of the grain structure, resulting in dramatic increment in average grain size of annealed AISI 304L foil. As the grain size is considerably larger, the grain fraction at specimen surface is much higher in the annealed specimen. These grains can deform more easily due to the reduced constraints at the surface. This is one of the reasons the annealed 304L specimen had a stress-strain curve with an obviously lower yield stress and flow stress followed by a smaller fracture strain.

Different from AISI 304L foil, the as-received AISI 439 foil material had a strong {111} macrotexture. The true stress-strain curve of as-received AISI 439 foil specimens in the transverse direction is about several degrees higher compared with the curves obtained from as-received AISI 304L foil specimens aligned to the rolling direction.

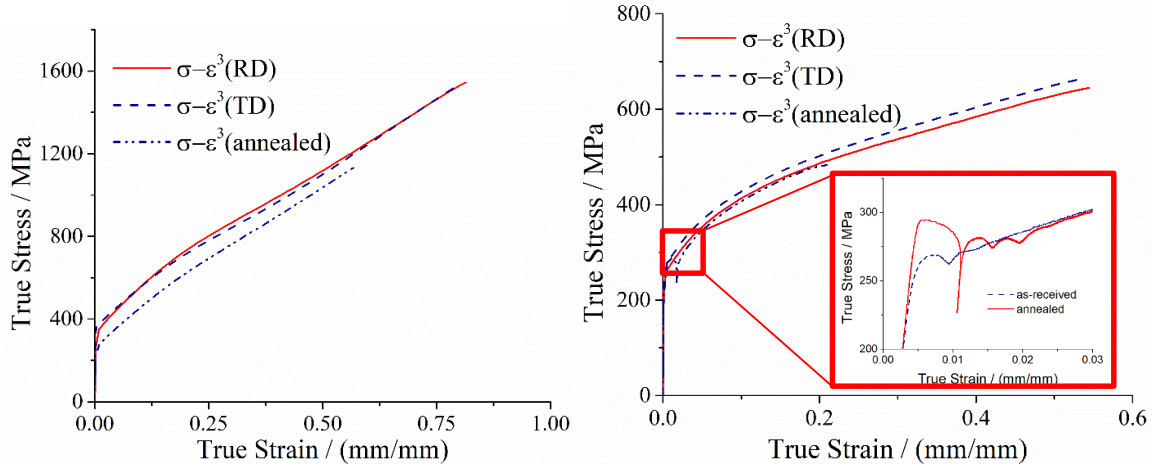

a b

Fig. 8 Effects of specimen microstructure on true stress-strain relations of a) AISI 304L and b) AISI 439 foils. The yielding phenomenon of annealed AISI439 foil specimens is shown as the subplot in b)

The fracture strain of annealed AISI 439 foil specimen is much smaller than the as-received specimens. Based on DIC measurement, plastic deformation of annealed AISI 439 foil specimen concentrated extensively within a small ellipse region (1.2 mm×1.8 mm) and was very small if outside the region. The maximum value of true plastic strain just prior to ductile fracture within this region was around 0.4, comparable to the as-received foil specimens in Table 2. This large strain inside the region was averaged out along the narrowest cross-section as Eq. (2), which is about 4 times larger of the ellipse size.

Table 2

Mechanical properties of foil materials under uniaxial tension

Specimen Description	0.2% offset Yield Stress, MPa	True Strain at Rupture	True Stress at Rupture, MPa
AISI304L(RD)	325.1±10.2	0.834± 0.028	1597.7±60.4
AISI304L(TD)	325.9±5.7	0.806±0.008	1532.1±2.19
annealed AISI304L	254.3±8.9	0.557±0.014	1118.2±18.3
AISI439(RD)	263.1±10.6	0.562±0.023	649.5±7.21
AISI439(TD)	273.7±7.7	0.554±0.023	666.5±2.90
annealed AISI439	235.4±6.5[a]	0.225±0.021	486.3±4.31

[a] obtained from lower yielding points.

5. Conclusions

75 μm thick cold-rolled stainless-steel AISI 304L and 439 foils were tested by uniaxial tensile test. The mechanical behaviors of foil specimens aligned to rolling or transverse directions, and after heat treatment were analysed using DIC-based deformation measurement technique. Following conclusions are made.

The DIC deformation measurement technique can focus only on the interested gage section, and thus is able to exclude the system compliance and specimen deformation outside the gage section. The true stress-strain relations of foil specimens under uniaxial tension obtained from DIC measurement is more convinced compared to the results derived from crosshead displacement. Furthermore, the DIC-based local strain measurement method could extend the stress-strain behavior valid to strain level 1.33 or 2.23 times larger of the onset of diffuse necking for AISI 304L and 439 foils, respectively.

The microstructural characterizations show strong influences on the mechanical behavior of stainless-steel foil specimens. The anisotropic material behaviors of foil specimens are found closely related to material macrotexture. Randomly textured AISI 304L foil specimens in either rolling or transverse direction have almost coincident stress-strain relations. The as-received AISI 439 foil specimens in transverse direction have 3-4 % higher flow stress compared to specimens in rolling direction because of its strong {111} texture. Due to obvious grain size increment after heat treatment, the stress-strain relation of annealed AISI 304L specimen is 2-3 % lower than the as-received ones.

The ductile fracture of AISI 304L foil specimens is dominant by tensile failure mode. The void nucleation and growth are well developed even though experienced a very short loading stage from peak load to the final fracture. Shear failure is found predominant in AISI 439 foil specimens due to serve shearing in the localized necking band.

Acknowledgments

This research was financial supported by Hefei University (No.17ZR01ZDA, 2018ZS01).

References

1. **Farbaniec, L.; Couque, H.; Dirras, G.** 2017. Size effects in micro-tensile testing of high purity polycrystalline nickel, Int. J. Eng. Sci. 119: 192-204. https://doi.org/10.1016/j.ijengsci.2017.06.016.
2. **Meng, B.; Fu, M. W.** 2015. Size effect on deformation behavior and ductile fracture in microforming of pure copper sheets considering free surface roughening, Mater. Design 83: 400-412. https://doi.org/10.1016/j.matdes.2015.06.067.
3. **Wang, S.; Niu, L.; Chen, C.; Pang, Y.** 2018. Size effects on the tensile properties and deformation mechanism of commercial pure titanium foils, Mat. Sci. Eng. A-Struct. 730: 244-261. https://doi.org/10.1016/j.msea.2018.06.009.
4. **Xu, Z.T.; Peng, L.F.; Lai, X.M.; Fu, M.W.** 2014. Geometry and grain size effects on the forming limit of sheet metals in msicro-scaled plastic deformation, Mat. Sci. Eng. A-Struct. 611: 345-353. https://doi.org/10.1016/j.msea.2014.05.060.
5. **Sergueeva, A. V.; Zhou, J.; Meacham, B. E.; Branagan, D. J.** 2009. Gage length and sample size effect on measured properties during tensile testing, Mat. Sci. Eng. A-Struct. 526(1-2): 79-83. https://doi.org/10.1016/j.msea.2009.07.046.
6. **Zhao, Y. H.; Guo, Y. Z.; Wei, Q.; Topping, T. D.; Dangelewicz, A. M.; Zhu, Y. T.; Lavernia, E. J.** 2009. Influence of specimen dimensions and strain measurement methods on tensile stress–strain curves, Mat. Sci. Eng. A-Struct. 525(1-2): 68-77. https://doi.org/10.1016/j.msea.2009.06.031.
7. **Chan, W. L.; Fu, M. W.** 2011. Experimental studies and numerical modeling of the specimen and grain size effects on the flow stress of sheet metal in micro-forming, Mat. Sci. Eng. A-Struct. 528(25-26): 7674-7683. https://doi.org/10.1016/j.msea.2011.06.076.
8. **Li, R.; Xin, R.; Liu, Q.; Chapuis, A.; Liu, S.; Fu, G.; Zong, L.** 2017. Effect of grain size, texture and density of precipitates on the hardness and tensile yield stress of Mg-14Gd-0.5 Zr alloys, Mater. Design. 114: 450-458. https://doi.org/10.1016/j.matdes.2016.10.074.
9. **Zhu, K. N.; Godfrey, A.; Hansen, N.; Zhang, X. D.** 2017. Microstructure and mechanical strength of near-

and sub-micrometre grain size copper prepared by spark plasma sintering, Mater. Design. 117: 95-103. https://doi.org/10.1016/j.matdes.2016.12.042.
10. **Chen, Y.; Kraft, O.; Walter, M.** 2015. Size effects in thin coarse-grained gold microwires under tensile and torsional loading, Acta. Mater. 87: 78-85. https://doi.org/10.1016/j.actamat.2014.12.034.
11. **Yang, L.; Lu, L.** 2013. The influence of sample thickness on the tensile properties of pure Cu with different grain sizes, Scripta. Mater. 69(3): 242-245. https://doi.org/10.1016/j.scriptamat.2013.04.009.
12. **Keller, C. Hug, E.** 2017. Kocks-Mecking analysis of the size effects on the mechanical behavior of nickel polycrystals, Int. J. Plasticity 98: 106-122. https://doi.org/10.1016/j.ijplas.2017.07.003.
13. **Zhang, H.; Liu, J.; Sui, D.; Cui, Z.; Fu, M.W.** 2018. Study of microstructural grain and geometric size effects on plastic heterogeneities at grain-level by using crystal plasticity modeling with high-fidelity representative microstructures, Int. J. Plasticity 100: 69-89. https://doi.org/10.1016/j.ijplas.2017.09.011.
14. **Kim, J. H.; Serpantié, A.; Barlat, F.; Pierron, F.; Lee, M. G.** 2013. Characterization of the post-necking strain hardening behavior using the virtual fields method, Int. J. Solids. Struct. 50(24): 3829–3842. https://doi.org/10.1016/j.ijsolstr.2013.07.018.
15. **Wang, L.; Tong, W.** 2015. Identification of post-necking strain hardening behavior of thin sheet metals from image-based surface strain data in uniaxial tension tests", Int. J. Solids. Struct. 75: 12-31. https://doi.org/10.1016/j.ijsolstr.2015.04.038.
16. **Pan, B.; Qian, K.; Xie, H.; Asundi, A.** 2009. Two-dimensional digital image correlation for in-plane displacement and strain measurement: a review, Meas. Sci. Technol. 20(6): 062001. https://doi.org/10.1088/0957-0233/20/6/062001.
17. **Jobba, M.; Mishra, R. K.; Niewczas, M.** 2015. Flow stress and work-hardening behaviour of Al–Mg binary alloys, Int. J. Plasticity 65: 43-60. https://doi.org/10.1016/j.ijplas.2014.08.006.
18. **Zavattieri, P. D.; Savic, V.; Hector Jr, L. G.; Fekete, J. R.; Tong, W.; Xuan, Y.** 2009. Spatio-temporal characteristics of the Portevin–Le Châtelier effect in austenitic steel with twinning induced plasticity, Int. J. Plasticity 25(12): 2298-2330. https://doi.org/10.1016/j.ijplas.2009.02.008.
19. **Blaber, J.; Adair, B.; Antoniou, A.** 2015. Ncorr: open-source 2D digital image correlation matlab software, Exp. Mech. 55(6): 1105-1122. https://doi: 10.1007/s11340-015-0009-1.
20. **Tong, W.; Yao, H.; Xuan, Y.** 2011. An improved error evaluation in one-dimensional deformation measurements by linear digital image correlation, Exp. Mech. 51(9): 1019–1031. https://doi.org/10.1007/s11340-010-9423-6.
21. **Tao, H.; Tong, W.; Hector JR, L.G.; Zavattieri, P. D.** 2008. Uniaxial tensile and simple shear behavior of resistance spot-welded dual-phase steel joints, J. Mater. Eng. Perform. 17(4): 517-534. https://doi.org/10.1007/s11665-007-9170-8.
22. **Kang, J.; McDermid, J. R.; Bruhis, M.** 2013. Determination of the constitutive behaviour of AA6022-T4 aluminium alloy spot welds at large strains, Mat. Sci. Eng. A-Struct. 567: 95-100. https://doi.org/10.1016/j.msea.2012.07.014.
23. **Florea, R. S.; Bammann, D. J.; Yeldell, A.; Solanki, K. N.; Hammi, Y.** 2013. Welding parameters influence on fatigue life and microstructure in resistance spot welding of 6061-T6 aluminum alloy, Mater. Design 45: 456-465. https://doi.org/10.1016/j.matdes.2012.08.053.

L. Wang

UNIAXIAL TENSILE BEHAVIOR OF 75 μm THICK STAINLESS-STEEL FOILS

S u m m a r y

Accurate knowledge about tensile behavior of thin stainless-steel foils at micro/meso scale is of great importance for potential industrial applications. In this work, two 75μm thick AISI 304L and 439 stainless-steel foils were tested under uniaxial tension. Digital image correlation (DIC) based strain measurement method was applied to characterize the plastic deformation of foil specimen. The stress-strain relations of foil specimens were identified from DIC-based strain measurement and compared with the results derived from crosshead displacement. It is found that the applied DIC method can more precisely characterize the mechanical behaviors of foil materials at small size scale. Fracture surface of foil specimens were also characterized. The material microstructures are found have predominant effect on tensile behaviors of foil materials.

Keywords: stainless-steel foils, digital image correlation, stress-strain relation, microstructure.

Received May 22, 2019
Accepted June 02, 2020